

A Fluorogenic Probe for the Catalyst-Free Detection of Azide-Tagged Molecules

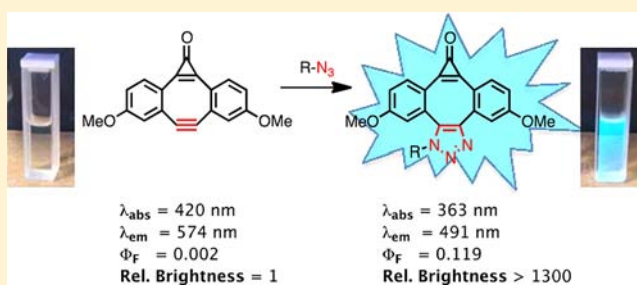
Frédéric Friscourt,[†] Christoph J. Fahrni,[‡] and Geert-Jan Boons^{*,†}

[†]Complex Carbohydrate Research Center, University of Georgia, 315 Riverbend Road, Athens, Georgia 30602, United States

[‡]School of Chemistry and Biochemistry and Petit Institute for Bioengineering and Bioscience, Georgia Institute of Technology, 901 Atlantic Drive, Atlanta, Georgia 30332, United States

S Supporting Information

ABSTRACT: Fluorogenic reactions in which non- or weakly fluorescent reagents produce highly fluorescent products can be exploited to detect a broad range of compounds including biomolecules and materials. We describe a modified dibenzocyclooctyne that under catalyst-free conditions undergoes fast strain-promoted cycloadditions with azides to yield strongly fluorescent triazoles. The cycloaddition products are more than 1000-fold brighter compared to the starting cyclooctyne, exhibit large Stokes shift, and can be excited above 350 nm, which is required for many applications. Quantum mechanical calculations indicate that the fluorescence increase upon triazole formation is due to large differences in oscillator strengths of the $S_0 \leftrightarrow S_1$ transitions in the planar C_{2v} -symmetric starting material compared to the symmetry-broken and nonplanar cycloaddition products. The new fluorogenic probe was successfully employed for labeling of proteins modified by an azide moiety.



INTRODUCTION

The selective and noninvasive labeling of biomolecules, ideally in context of their endogenous environment, is a prerequisite for a broad range of biological studies. As a genetically encoded label, the green fluorescent protein (GFP) and its variants have revolutionized cell biology by enabling the visualization of target proteins within live cells, tissues, and whole organisms.^{1–3} GFP is, however, not suitable for tagging metabolites and post-translationally modified biomolecules such as lipids, nucleic acids, and complex carbohydrates.

The bioorthogonal chemical reporter methodology, pioneered by Bertozzi and co-workers, is emerging as a versatile method for labeling a wide variety of biomolecules.^{4–6} In this approach, an abiotic chemical functionality (reporter) is incorporated into a target biomolecule, which can be reacted with a complementary bioorthogonal functional group linked to a diverse set of probes, including biotin and fluorescent tags. Organic azides are particularly versatile reporters due to their small size and virtual absence in biological systems.⁷ They can be conjugated by Staudinger ligation using modified phosphines,^{8,9} copper(I)-catalyzed cycloaddition with terminal alkynes (CuAAC),^{10–12} or by strain-promoted alkyne–azide cycloaddition (SPAAC).^{13,14} The latter type of reaction is attractive because it is fast and does not require a potentially toxic metal catalyst, thereby offering opportunities for the labeling of glycans, lipids and proteins in living cells, tissues or whole organisms. For example, Bertozzi and co-workers have shown that glycoconjugates of zebrafish embryos can be visualized by metabolic labeling with *N*-azidoacetylgalactos-

amine followed by cycloaddition with difluorinated cyclooctyne (DIFO) conjugated to a fluorophore.¹⁵

We have demonstrated that 4-dibenzocyclooctynol (DIBO) is an attractive reagent for SPAAC. It rapidly reacts with azido-containing compounds and can be employed for tagging a wide variety of biomolecules including cell surface glycoconjugates of living cells.¹⁶ Dibenzocyclooctynes can be readily derivatized, which was exploited to influence their subcellular location via incorporation of sulfates.¹⁷ Furthermore, the cycloadditions can be accelerated by modifying the 8-membered ring of DIBO with an sp^2 -hybridized atom.^{18–20} Dibenzocyclooctynes can also be generated photochemically by short irradiation with UV light of corresponding cyclopropenones, thereby making it possible to label target substrates in a spatially and temporally controlled manner.²¹ In addition to bioconjugation, SPAAC has found wide utility in materials and surface chemistry.²²

We envisaged that DIBO derivative **1**, which contains a reactive alkyne and an alkyne masked as a cyclopropenone, would offer an attractive bifunctional reagent for tagging biomolecules and materials under catalyst free conditions.²³ Although the sequential SPAAC did not proceed satisfactorily, we found that cycloaddition of **1** with azides yielded strongly fluorescent triazoles that possess favorable photophysical properties, such as exceptional brightness, a large Stokes shift, and excitation above 350 nm. Quantum mechanical calculations indicate that the fluorescence increase upon triazole formation

Received: September 10, 2012

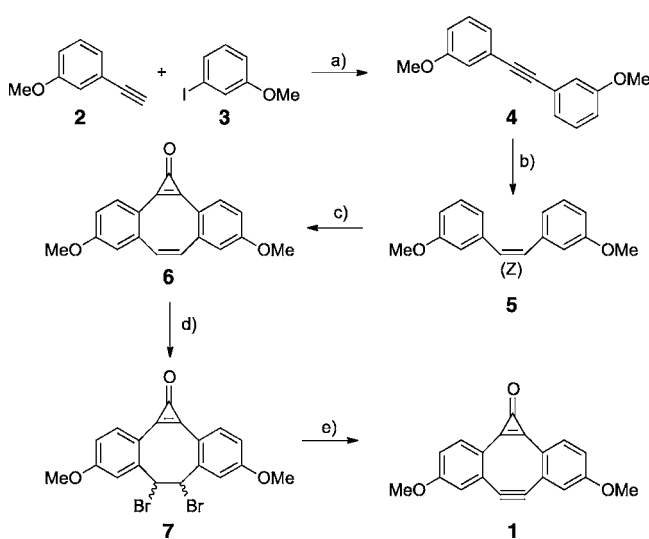
Published: October 24, 2012

is due to substantial differences in oscillator strengths of the $S_0 \leftrightarrow S_1$ transitions in the planar C_{2v} -symmetric Fl-DIBO (**1**) compared to the symmetry-broken and nonplanar cycloaddition products. Compounds that become fluorescent upon reaction with a chemical reporter have many attractive features such as eliminating the need for probe washout, reducing background labeling, offering opportunities for monitoring biological processes in real time.²⁴

RESULTS AND DISCUSSION

Synthesis of **1 and Cycloaddition to Azides.** The preparation of target compound **1** commenced by Sonogashira cross-coupling of 3-ethynylanisole (**2**) and 3-iodoanisole (**3**) to give the symmetrical ethyne **4** in near quantitative yield (Scheme 1). Partial hydrogenation of **4** using Lindlar's catalyst

Scheme 1. Synthesis of Fl-DIBO^a



^aReagents and conditions: (a) Pd(PPh₃)₄, CuI, (iPr)₂NEt, THF, reflux, 18 h, 97%; (b) H₂, Lindlar's catalyst, quinoline, hexane, rt, 20 min, 89%; (c) AlCl₃, tetrachlorocyclopropene, CH₂Cl₂, -20 °C to rt, 4 h, H₂O, 62%; (d) Br₂, CH₂Cl₂, 0 °C, 2 h, 87%; (e) KOH, EtOH, rt, 18 h, 76%.

produced Z-alkene **5**, and subsequent Friedel–Crafts alkylation with tetrachlorocyclopropene in the presence of AlCl₃^{21,25} yielded the corresponding annulated dichlorocyclopropene intermediate, which after in situ hydrolysis gave cyclopropenone derivative **6** in 62% overall yield. Selective bromination of the bridging double bond provided dibromocyclopropenone derivative **7**, which upon treatment with ethanolic KOH solution underwent a double-elimination reaction to give the target compound **1**. Despite the considerable strain imposed by the central ring system, compound **1** is stable in aqueous solution over a broad pH range and inert toward treatment with a diverse set of nucleophiles including glutathione (10 mM) (Supporting Information, Figures S2–S5).

Triazoles **8a–e** were obtained in near quantitative yield by cycloaddition of **1** with the corresponding azide derivatives in a mixture of dichloromethane and methanol (4:1, v/v) at room temperature in the course of 2 h (Figure 1a). The progress of the reaction of **1** with benzyl azide in a mixture of CDCl₃ and CD₃OD (4:1, v/v) was monitored by ¹H NMR by integration of the benzylic proton signals, and yielded a second-order rate

constant of 0.019 M⁻¹ s⁻¹ (Supporting Information, Figure S1). The reaction rate is somewhat lower than that of the parent DIBO (0.057 M⁻¹ s⁻¹) indicating that the cyclopropenone moiety does not induce additional ring strain.²⁶

Photophysical Properties. An unexpected and exciting observation was the strong fluorescence increase upon conversion of the Fl-DIBO (**1**) probe to the corresponding triazole products **8a–e** (Figure 1b). Thus, excitation of Fl-DIBO **1** at 420 nm produces only a weak emission band centered around 574 nm with a low quantum yield of 0.2% (Table 1 and Figure 1b). In contrast, triazole **8a**, which was obtained by cycloaddition of **1** with triethyleneglycol methyl monoester azide, fluoresces strongly upon excitation at 370 nm with a maximum intensity at 491 nm and a quantum yield of 11.9% (Table 1 and Figure 1b). Because of the large difference in the extinction coefficients of Fl-DIBO (**1**) ($\epsilon_{420 \text{ nm}} = 190 \text{ M}^{-1} \text{ cm}^{-1}$) and the triazole product **8a** ($\epsilon_{370 \text{ nm}} = 4300 \text{ M}^{-1} \text{ cm}^{-1}$), the apparent brightness, defined as the product of quantum yield and molar absorption coefficient, is more than 1000-fold increased. Whereas many common fluorophores including fluorescein, rhodamine, or BODIPY derivatives exhibit small Stokes shifts that may cause reabsorption of emitted photons, triazole **8a** possesses an unusually large Stokes shift of 7180 cm⁻¹ (128 nm).

More detailed examination of compounds **8a–e** revealed that the nature of the triazole substituent does not substantially affect the photophysical properties (Table 1 and Supporting Information, Figures S8–S18). Only compound **8c** showed a significant red-shift of the emission maximum along with a reduced quantum yield and shorter fluorescence lifetime, presumably due to direct π -interaction of the anisole substituent with the fluorophore core π -system. The radiative deactivation rate constants of **8a–e**, calculated from the fluorescence quantum yields and lifetimes, are narrowly distributed with an average of $1.13 \pm 0.16 \times 10^7 \text{ s}^{-1}$, suggesting a single and uniform deactivation pathway.

Furthermore, compounds **8a–e** showed a pronounced negative solvatochromism, indicating a less polar excited state compared to the ground state. For example, the emission maximum of benzyl triazole **8b** moved from 493 nm in toluene to 482 nm in methanol (Supporting Information, Figure S7). Finally, treatment of the triazole **8b** (10⁻⁵ M in MeOH) with glutathione (10 mM) for 2 h resulted in marginal bleaching. Strong reducing agents such as DTT caused, however, complete bleaching within 30 min, probably by addition of DDT to the cyclopropenone moiety of **8b** (Supporting Information, Figure S6).

Protein Labeling. Next, Fl-DIBO (**1**) was examined as a fluorogenic labeling reagent for proteins. For this purpose, bovine serum albumin (BSA) was modified with an azide moiety by reaction of the Cys34 sulfhydryl group with *N*-{2-[2-(2-azidoethoxy)ethoxy]ethyl}-2-iodoacetamide to give **9** (Supporting Information). A stock solution of Fl-DIBO (**1**) in ethanol was then added to a solution of BSA-azide (**9**) in PBS containing 1% SDS and the resulting reaction mixture was incubated at 37 °C for 18 h. An aliquot was analyzed by SDS-PAGE followed by fluorescence imaging and staining with Coomassie Blue for protein detection (Figure 2, lane 1). As expected, a strong fluorescent band was observed at 66 kDa. As negative controls, Fl-DIBO was excluded (lane 3), or BSA-azide replaced by unmodified BSA (lane 2) and, gratifyingly, the fluorescent images showed an absence of background labeling. As an additional control, BSA-azide was exposed to DIBO-

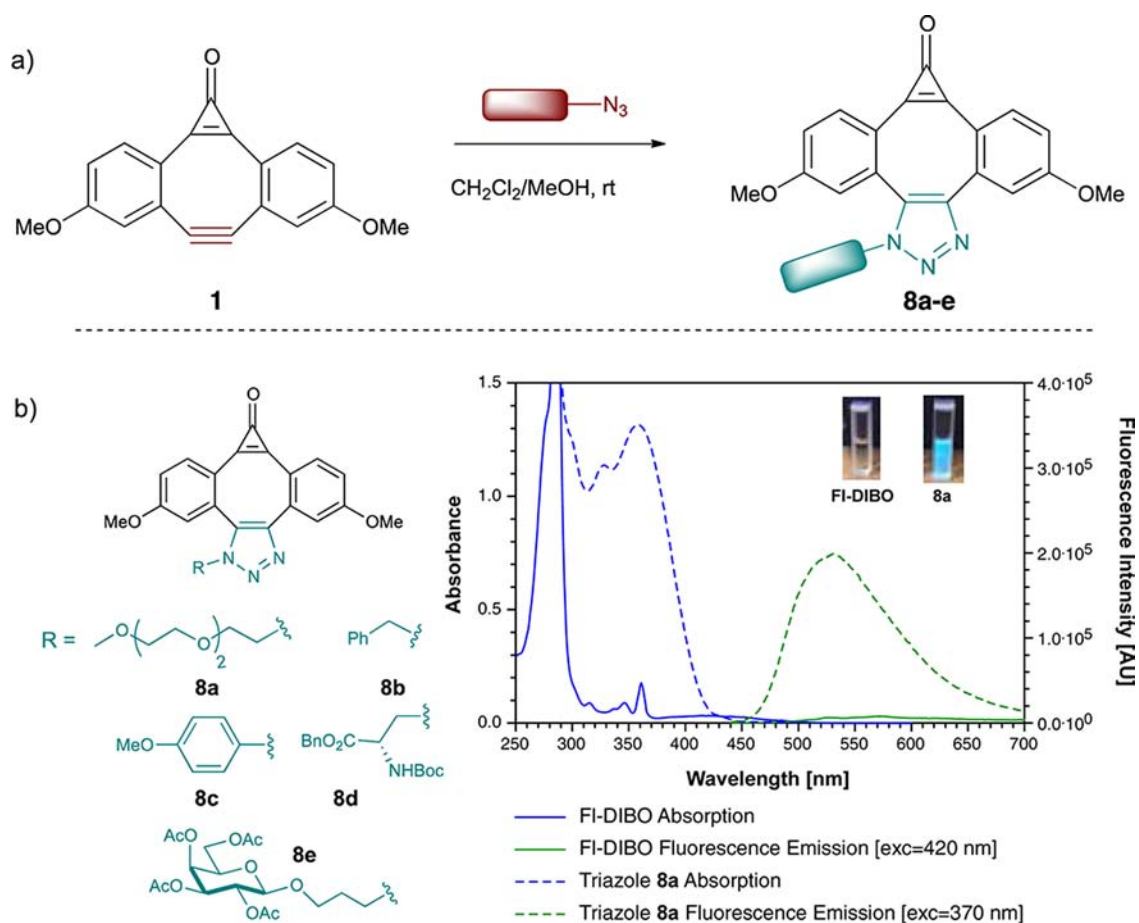


Figure 1. (a) SPAAC between FI-DIBO probe (**1**) and various azides; (b) various triazole products generated from the corresponding azides with FI-DIBO probe; absorption (solid blue trace) and emission (solid green trace, $\lambda_{\text{exc}} = 420$ nm) spectra of FI-DIBO and absorption (dashed blue trace) and emission (dashed green trace, $\lambda_{\text{exc}} = 370$ nm) spectra of triethyleneglycol triazole **8a** recorded in MeOH. Inset images compare the visible fluorescence emission of the FI-DIBO probe (left cuvette) to the triazole product (**8a**) (right cuvette) under UV excitation (365 nm).

Table 1. Photophysical Properties of FI-DIBO (1**) and Triazoles **8a–e** in Methanol at 298 K**

compound	1	8a	8b	8c	8d	8e
λ_{abs} [nm]	420	363	364 ^e	366	360	362
ϵ_{abs} [$\text{M}^{-1} \text{cm}^{-1}$] ^a	190	4300	4600	1700	5000	6100
λ_{em} [nm]	574	491	489	499	492	489
Stokes shift [cm^{-1}]	6390	7180	7020	7280	7450	7170
Φ_{F} ^b	0.002	0.119	0.12	0.065	0.087	0.12
Life time [ns] ^c	1.61 ± 0.01^f	9.55 ± 0.01	8.59 ± 0.01^g	7.10 ± 0.01^h	8.81 ± 0.01	9.80 ± 0.01
k_{r} [10^7 s^{-1}] ^d	0.12	1.25	1.16	0.92	0.99	1.22

^aDetermined at 420 nm for **1** and at 370 nm for **8a–e**. ^bFluorescence quantum yield, quinine sulfate in 1.0 N H_2SO_4 as standard. ^cFluorescence decay acquired at 490 nm and fitted to a monoexponential decay model. ^dRadiative deactivation rate constant ($k_{\text{r}} = \Phi_{\text{F}}/\tau_{\text{F}}$). ^eMaximum of excitation spectrum. ^fNatural decay lifetime based on biexponential decay with $\tau_1 = 0.51$ ns (62%) and $\tau_2 = 3.40$ ns (38%). ^gNatural decay lifetime based on biexponential decay with $\tau_1 = 9.43$ ns (88%) and $\tau_2 = 2.41$ ns (12%). ^hAcquired at 500 nm.

FITC and after appropriate washing steps a fluorescent band was observed at 66 kDa (lane 4). A similar reaction with unmodified BSA (lane 5) showed faint background labeling, thus highlighting superior properties of **1**.^{27,28}

Computational Studies. The unexpected and large increase in quantum yield upon conversion of FI-DIBO (**1**) to the triazoles **8a–e** prompted us to explore the underpinning mechanism by quantum chemical calculations. The fluorescence switching of previously reported fluorogenic CuAAC reagents^{24,29–31} can be rationalized by considering the relative energy levels of the emissive singlet $^1(\pi-\pi^*)$ -excited state and a quenching triplet $^3(n-\pi^*)$ -state,³² which is typically the lowest

excited state in azido-substituted fluorophores.³³ Upon conversion to the triazole, the quenching $^3(n-\pi^*)$ -state rises above the emissive $^1(\pi-\pi^*)$ -state and the fluorescence is switched on. A similar excited state inversion mechanism is also responsible for the fluorogenic response of an alkyne-substituted coumarin derivative.²⁹ In this case, triazole formation increases the charge-transfer character of the emissive $^1(\pi-\pi^*)$ -state, which in polar solvents is sufficiently stabilized to move below the quenching $^3(n-\pi^*)$ -state. Similar to coumarins, excitation of the carbonyl lone-pair electrons in FI-DIBO (**1**) could yield an energetically low-lying $^3(n-\pi^*)$ -state, which upon conversion to the triazoles might then rise

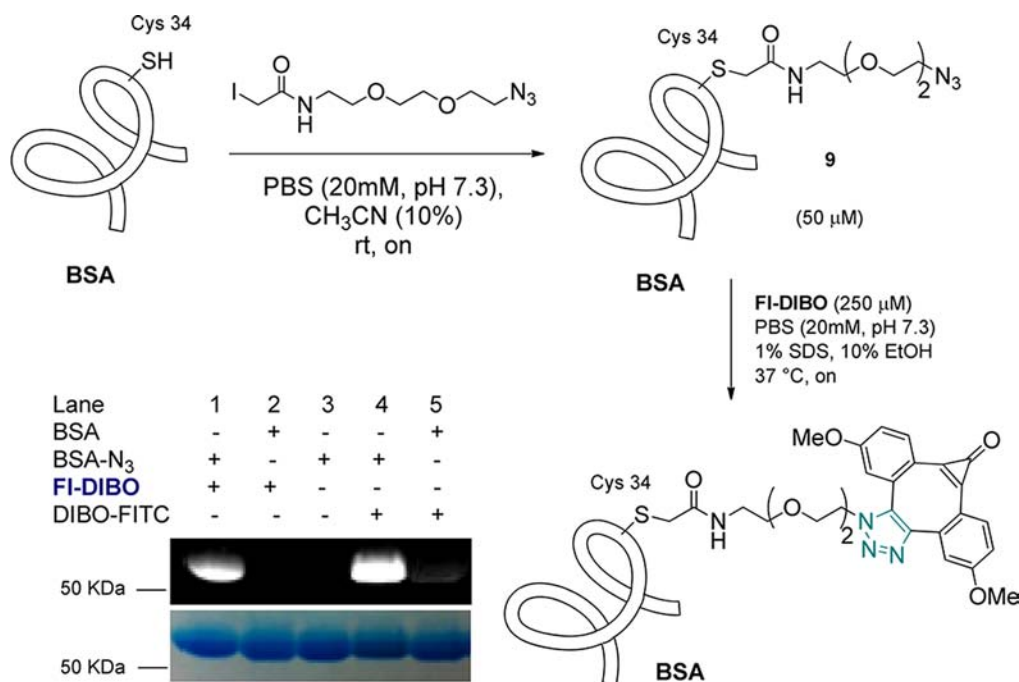


Figure 2. Formation of azido-BSA and its labeling with FI-DIBO probe. Purified azido-BSA (50 μM) and native BSA (50 μM) were labeled with 250 μM of FI-DIBO (**1**) or DIBO-FITC for 18 h at 37 $^{\circ}\text{C}$ in PBS containing 10% EtOH and 1% SDS. The crude reaction mixtures were separated by SDS-PAGE and the gel was analyzed by fluorescence imaging (top row; $\lambda_{\text{exc}} = 365 \text{ nm}$; $\lambda_{\text{detec}} = 480 \text{ nm}$) and by Coomassie Blue stain to reveal total protein content (bottom row).

Table 2. Computational Data for FI-DIBO (1**) and Triazole **8f** ($\text{R} = \text{CH}_3$)^a**

compd	data	exp ^b	state	TD-B3LYP/6-31+G(d) gasphase	TD-B3LYP/6-31+G(d) PCM ^d	TD-CAM-B3LYP/6-31+G(d) PCM ^d
1	absorption [eV] ^c	2.95	$S_1 (\pi-\pi^*)$	2.60 (0.014)	2.60 (0.023)	2.95 (0.023)
			$S_2 (n-\pi^*)$	2.79 (0.0001)	3.24 (0.0002)	4.01 (0.0003)
	emission [eV]	2.16	$S_1 (\pi-\pi^*)$	1.78 (0.007)	1.82 (0.011)	2.06 (0.011)
		E_{00} [eV] ^e	2.56		2.19	2.21
8f	absorption [eV] ^c	3.41	$S_1 (\pi-\pi^*)$	3.17 (0.093)	3.23 (0.18)	3.65 (0.23)
			$S_2 (n-\pi^*)$	3.27 (0.0152)	3.68 (0.0123)	4.37 (0.028)
	emission [eV]	2.53	$S_1 (\pi-\pi^*)$	2.13 (0.026)	2.26 (0.058)	2.56 (0.071)
		E_{00} [eV] ^e	3.06		2.65	2.75
	MAE [eV] ^f			0.36	0.30	0.08

^aAll geometries were optimized at the B3LYP/6-31G(d) level of theory. ^bLowest energy absorption band maximum of **8a** in methanol. ^cVertical excitation energy; oscillator strength in parentheses. ^dPolarized continuum model with methanol as solvent. ^eExcited state equilibrium energy. ^fMean absolute error.

above the emissive $^1(\pi-\pi^*)$ -level. To explore this scenario, we calculated the excited state manifold of FI-DIBO (**1**) and the corresponding methyl-substituted triazole product **8f** by TD-DFT at the B3LYP/6-31+G(d)//B3LYP/6-31G(d) level of theory and gauged the validity of the computational results based on the experimental absorption and emission data. As evident from the data compiled in Table 2, the vertical excitation and emission energies were underestimated by an average of 0.39 eV, a value that falls within the error margin of previous benchmark tests of TD-DFT/B3LYP.³⁴ Accounting for solvent effects with a polarized continuum model (PCM) yielded further improved values, and switching to the long-range corrected hybrid functional CAM-B3LYP³⁵ reproduced the experimental data very well with a low average error of 0.08 eV. Although the vertical excitation energy is not a measurable quantity as the electronic spectrum is further resolved into vibrational bands, the experimental absorption maximum for symmetry-allowed transitions lies usually close to the vertical excitation energy,³⁶ and thus may still serve as a meaningful

gauge. As illustrated with the electron density difference plots and the state energy diagram in Figure 3, the lowest energy absorption and emission bands correspond to $^1(\pi-\pi^*)$ states, both for FI-DIBO (**1**) and the triazole **8f**. Furthermore, the $^1(n-\pi^*)$ state of FI-DIBO (**1**) resides by more than 1 eV above the emissive $^1(\pi-\pi^*)$ state, suggesting that nonradiative deactivation via a $^1(\pi-\pi^*) \rightarrow ^3(\pi-\pi^*)$ route is unlikely responsible for the low quantum yield. Within the C_{2v} -symmetric molecular framework, the two states have B_2 and B_1 symmetry, respectively, thus rendering such a deactivation pathway also symmetry-forbidden. Given the rigid molecular architecture of FI-DIBO (**1**), excited state deactivation pathways that require large structural changes, for example, via a conical intersection to a lower-lying triplet state, appear also improbable. Rather, the low quantum yield of FI-DIBO (**1**) likely originates from the much weaker oscillator strengths and lower energy associated with the $S_0 \leftrightarrow S_1$ transitions compared to the triazoles **8**. According to classical theory, the radiative rate constant k_r for emission is proportional to the product of

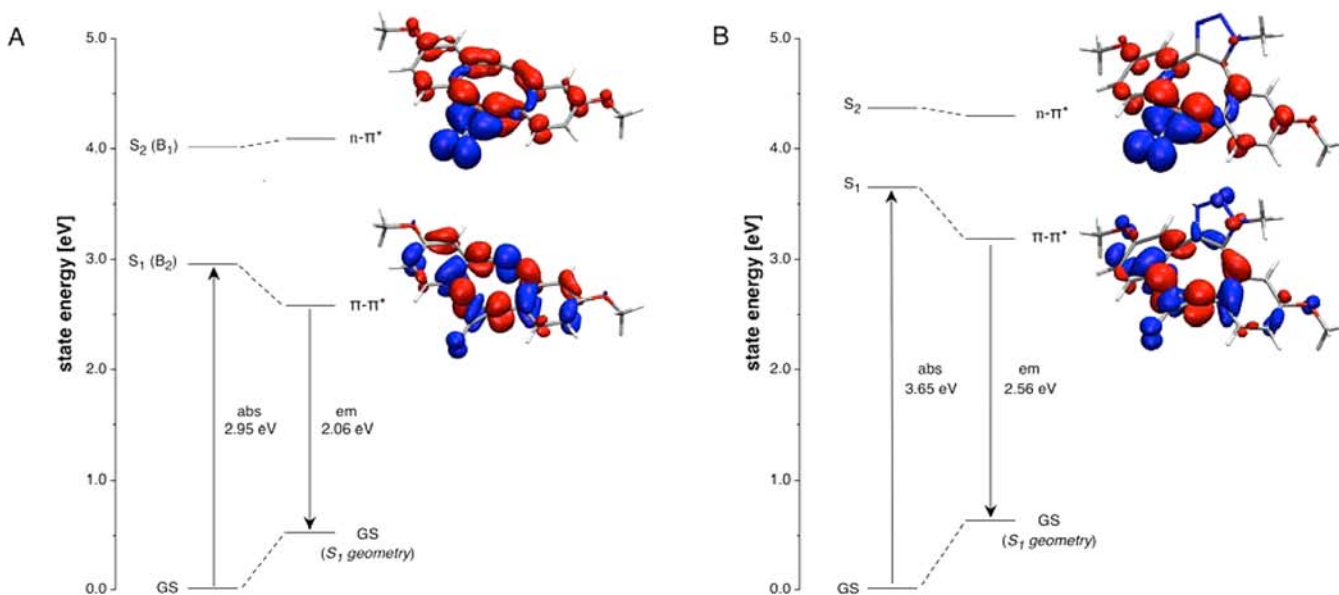


Figure 3. Excited state manifold for (A) Fl-DIBO (**1**) and (B) the triazole **8f** illustrating the relative energies of the $^1(\pi-\pi^*)$ and $^1(n-\pi^*)$ singlet states in methanol (TD-DFT at the CAM-B3LYP/6-31+G(d)//B3LYP/6-31G(d) level of theory, including PCM solvent correction). The color plots illustrate the total electron density difference between the respective ground and excited states (decreasing density shown in blue, increasing density red; GS = ground state; S_1 , S_2 = first and second excited singlet state).

the oscillator strength and the squared state energy.³⁷ On the basis of the data in Table 2, k_f is expected to be approximately 13-times slower for **1** compared to **8f**, a value that mirrors well the experimental data (Table 1).

On the basis of an extensive set of structural and computational data, it was recently suggested that the alkyne bond angle in cyclooctyne derivatives may serve as a predictor for their reactivity.³⁸ Consistent with this proposal, the alkyne bond angles in the ground state equilibrium geometry of Fl-DIBO (**1**) are 156° , thus implying a reduced ring strain compared to the more reactive biarylazacyclooctynone derivative BARAC with alkyne bond angles of 153° .³⁸

CONCLUSIONS

Bioorthogonal fluorogenic reactions in which non- or weakly fluorescent reagents produce highly fluorescent products greatly expand the possibilities for detecting a broad range of compounds and are particularly advantageous for applications in which probe washout is not possible or desirable.²⁴ A number of such probes have been developed by modifying common fluorophore platforms such as anthracene, BODIPY, or coumarins with an azide moiety as quencher.^{29–31,39,40} Upon Cu(I)-catalyzed cycloaddition to an alkyne-tagged target molecule, the quenching azide is converted to a triazole and the fluorophore emission restored. While in principle the same approach could be used for strain-promoted cycloadditions, the corresponding tags would be inevitably much larger compared to the rather inconspicuous propargyl groups used in CuAAC, and the increased molecular size might adversely affect the properties of smaller target molecules, especially with regard to their biodistribution and biological activity. For this reason, the preferred approach for developing a catalyst-free fluorogenic click reagent is to utilize azide as the tagging moiety and to integrate the strained and bulky cyclooctyne group into the fluorophore structure. A first attempt toward this goal was recently reported by Bertozzi and co-workers, who designed the fluorogenic reagent CoumBARAC by fusing the cyclooctyne

ring with a coumarin fluorophore.⁴¹ Although the reaction product with 2-azidoethanol exhibited a 10-fold increased emission compared to unreacted CoumBARAC, it exhibited a low fluorescence quantum yield and required excitation at 300 nm, a wavelength regime that is incompatible with many biological applications. In contrast, the cycloaddition product of Fl-DIBO (**1**) is more than 1000-fold brighter compared to the unreacted reagent, offers a large Stokes shift, and can be excited above 350 nm, the typical cutoff wavelength of standard fluorescence microscopes. Quantum mechanical calculations indicate that the fluorescence increase upon triazole formation is not due to a $(n-\pi^*)/(\pi-\pi^*)$ inversion mechanism as found in previous probes but rather related to the substantial differences in oscillator strengths of the $S_0 \leftrightarrow S_1$ transitions in the planar C_{2v} -symmetric Fl-DIBO (**1**) compared to the symmetry-broken and nonplanar cycloaddition products. Because the fluorescence switching mechanism does not rely on the alteration of excited state energy levels, the turn-on response of Fl-DIBO (**1**) is very robust and virtually independent from the polarity of the surrounding environment, thus eliminating the potential for artifacts in complex biological samples. Compared to previously reported fluorogenic click reagents, Fl-DIBO (**1**) does not require a metal-catalyst for bioconjugation while still maintaining rapid reaction kinetics. Given these favorable properties, Fl-DIBO (**1**) represents a significant advance and is expected to facilitate fluorescent labeling of biomolecules and materials while eliminating the problem of background labeling and need of washing steps. The proposed fluorescent turn-on mechanism will offer unique opportunities to design additional fluorogenic probes with modified properties.

EXPERIMENTAL SECTION

Bis(3-methoxyphenyl)acetylene (4). *N,N*-Diisopropylethylamine (1.5 mL, 9.0 mmol) was added dropwise to a solution of 3-ethynylanisole (0.45 mL, 3.6 mmol), 3-iodoanisole (0.36 mL, 3.0 mmol), tetrakis(triphenylphosphine)palladium(0) (170 mg, 0.15 mmol) and copper(I) iodide (60 mg, 0.3 mmol) in THF (15 mL).

The reaction mixture was then refluxed overnight. After being cooled to room temperature, all volatiles were removed under reduced pressure. The residue was then purified by flash column chromatography on silica gel using a mixture of hexane and ethyl acetate (8:1) affording pure alkyne **4** as a colorless solid (694 mg, 97%): $^1\text{H NMR}$ (300 MHz, CDCl_3): δ 3.82 (s, 6H), 6.89 (dd, $J = 7.8, 2.0$ Hz, 2H), 7.06 (br s, 2H), 7.13 (d, $J = 7.8$ Hz, 2H), 7.25 (t, $J = 7.8$ Hz, 2H); $^{13}\text{C NMR}$ (75.5 MHz, CDCl_3): δ 55.44 ($2 \times \text{CH}_3$), 89.26 ($2 \times \text{C}$), 115.15 ($2 \times \text{CH}$), 116.49 ($2 \times \text{CH}$), 124.31 ($2 \times \text{C}$), 124.35 ($2 \times \text{CH}$), 129.55 ($2 \times \text{CH}$), 159.50 ($2 \times \text{C}$); HRMS (m/z): $[\text{M}^+]$ calcd. for $\text{C}_{16}\text{H}_{14}\text{O}_2$, 238.0994; found, 238.0971.

(Z)-3,3'-Dimethoxystilbene (5). A solution of alkyne **4** (672 mg, 2.82 mmol), Lindlar's catalyst (135 mg, 20% w/w) and quinoline (0.72 mL, 6.1 mmol) in hexane (17 mL) was stirred at room temperature under 1 atm of H_2 for 20 min. The mixture was then filtered through Celite and washed with ethyl acetate (20 mL). The filtrate was then concentrated under reduced pressure and the residue was purified by flash column chromatography on silica gel using a mixture of hexane and ethyl acetate (8:1) affording pure (Z)-alkene **5** as a colorless oil (604 mg, 89%): $^1\text{H NMR}$ (300 MHz, CDCl_3): δ 3.64 (s, 6H), 6.57 (s, 2H), 6.73 (dd, $J = 7.9, 2.5$ Hz, 2H), 6.80 (br s, 2H), 6.84 (d, $J = 7.9$ Hz, 2H), 7.14 (t, $J = 7.9$ Hz, 2H); $^{13}\text{C NMR}$ (75.5 MHz, CDCl_3): δ 55.15 ($2 \times \text{CH}_3$), 113.41 ($2 \times \text{CH}$), 113.93 ($2 \times \text{CH}$), 121.62 ($2 \times \text{CH}$), 129.31 ($2 \times \text{CH}$), 130.46 ($2 \times \text{CH}$), 138.65 ($2 \times \text{C}$), 159.49 ($2 \times \text{C}$); HRMS (m/z): $[\text{M}^+]$ calcd. for $\text{C}_{16}\text{H}_{16}\text{O}_2$, 240.1150; found, 240.1109.

4,9-Dimethoxy-1H-dibenzo[a,e]cyclopropa[c]cycloocten-1-one (6). A solution of aluminum chloride (400 mg, 3.0 mmol) and tetrachlorocyclopropene (0.15 mL, 1.2 mmol) in CH_2Cl_2 (15 mL) was stirred at room temperature for 20 min. The reaction mixture was then cooled to -20°C and a solution of (Z)-alkene **5** (240 mg, 1.0 mmol) in CH_2Cl_2 (5 mL) was added. The reaction mixture was stirred at -20°C for 1 h, was then allowed to warm to room temperature over a period of 2 h and was stirred for an extra h at room temperature. Water (20 mL) was then added and the reaction mixture was stirred for an extra 30 min. The organic layer was then extracted with CH_2Cl_2 (3×20 mL), dried over MgSO_4 and concentrated under reduced pressure. The residue was then purified by flash chromatography on silica gel (16 g) using a mixture of 2% MeOH in CH_2Cl_2 affording pure cyclopropenone **6** (180 mg, 62%) as a yellow/orange solid: $^1\text{H NMR}$ (300 MHz, CDCl_3): δ 3.82 (s, 6H), 5.99 (s, 2H), 6.60 (d, $J = 2.5$ Hz, 2H), 6.69 (dd, $J = 8.4, 2.5$ Hz, 2H), 7.44 (d, $J = 8.4$ Hz, 2H); $^{13}\text{C NMR}$ (75.5 MHz, CDCl_3): δ 55.66 ($2 \times \text{CH}_3$), 113.45 ($2 \times \text{CH}$), 115.34 ($2 \times \text{C}$), 121.75 ($2 \times \text{CH}$), 131.87 ($2 \times \text{CH}$), 136.13 ($2 \times \text{CH}$), 140.01 ($2 \times \text{C}$), 147.73 ($2 \times \text{C}$), 152.39 (C=O), 163.52 ($2 \times \text{C}$); HRMS (m/z): $[\text{M} + \text{H}^+]$ calcd. for $\text{C}_{19}\text{H}_{15}\text{O}_3$, 291.1016; found, 291.1011.

6,7-Dibromo-4,9-dimethoxy-6,7-dihydro-1H-dibenzo[a,e]cyclopropa[c]cycloocten-1-one (7). A solution of bromine (48 μL , 0.93 mmol) in CH_2Cl_2 (4 mL) was added dropwise to a solution of cyclopropenone **6** (180 mg, 0.62 mmol) in CH_2Cl_2 (8 mL) at 0°C . The reaction mixture was allowed to warm to room temperature and was stirred for 4 h. The mixture was then quenched with a saturated aqueous solution of sodium thiosulfate (10 mL). The two phases were then separated and the aqueous layer was further extracted with CH_2Cl_2 (3×10 mL). The combined organic extracts were dried over MgSO_4 , filtered and concentrated under reduced pressure. The residue was then purified by flash chromatography on silica gel (16 g) using a mixture of 2% MeOH in CH_2Cl_2 affording pure dibromo-cyclopropenone **7** (243 mg, 87%) as a colorless solid: $^1\text{H NMR}$ (300 MHz, CDCl_3): δ 3.91 (s, 6H), 5.75 (s, 2H), 6.97 (d, $J = 2.5$ Hz, 2H), 7.05 (dd, $J = 8.5, 2.5$ Hz, 2H), 8.06 (d, $J = 8.5$ Hz, 2H); $^{13}\text{C NMR}$ (75.5 MHz, CDCl_3): δ 50.44 ($2 \times \text{CH}$), 55.88 ($2 \times \text{CH}_3$), 114.14 ($2 \times \text{CH}$), 115.71 ($2 \times \text{C}$), 118.24 ($2 \times \text{CH}$), 137.16 ($2 \times \text{CH}$), 141.74 ($2 \times \text{C}$), 142.96 ($2 \times \text{C}$), 152.71 (C=O), 162.72 ($2 \times \text{C}$); HRMS (m/z): $[\text{M}^+]$ calcd. for $\text{C}_{19}\text{H}_{14}\text{O}_3^{79}\text{Br}_2$, 447.9310; found, 447.9313.

4,9-Dimethoxy-6,7-didehydro-1H-dibenzo[a,e]cyclopropa[c]cycloocten-1-one (1). A solution of potassium hydroxide (300 mg, 5.30 mmol) in ethanol (5 mL) was added to a solution of dibromo-cyclopropenone **7** (240 mg, 0.53 mmol) in ethanol (25 mL).

The reaction mixture was then stirred at room temperature overnight. The solution was quenched with an aqueous solution of HCl (1N, until $\text{pH} \approx 6$). The mixture was then extracted with CH_2Cl_2 (3×10 mL) and the combined organic extracts were dried over MgSO_4 , filtered and concentrated under reduced pressure. The residue was then purified by flash chromatography on silica gel (16 g) using a mixture of 1% MeOH in CH_2Cl_2 affording pure cyclooctyne **1** (116 mg, 76%) as a yellow solid: $^1\text{H NMR}$ (300 MHz, CDCl_3): δ 3.80 (s, 6H), 6.45 (d, $J = 2.5$ Hz, 2H), 6.63 (dd, $J = 8.5, 2.5$ Hz, 2H), 7.47 (d, $J = 8.5$ Hz, 2H); $^{13}\text{C NMR}$ (75.5 MHz, CDCl_3): δ 55.81 ($2 \times \text{CH}_3$), 106.82 ($2 \times \text{C}$), 113.70 ($2 \times \text{CH}$), 114.80 ($2 \times \text{CH}$), 125.38 ($2 \times \text{C}$), 126.87 ($2 \times \text{C}$), 136.76 ($2 \times \text{CH}$), 146.48 ($2 \times \text{C}$), 153.81 (C=O), 163.39 ($2 \times \text{C}$); HRMS (m/z): $[\text{M} + \text{H}^+]$ calcd. for $\text{C}_{19}\text{H}_{13}\text{O}_3$, 289.0859; found, 289.0813.

General Procedure for Triazole Formation. A solution of Fl-DIBO **1** (14.4 mg, 0.05 mmol) and the respective azide **10a**, **10b** (BnN_3), **10c**, **10d**, and **10e** (0.1 mmol) in a mixture of CH_2Cl_2 and methanol (4:1, 5 mL) was stirred at room temperature for 2 h. All volatiles were removed under reduced pressure and the residue was purified by flash chromatography on silica gel (7 g) using an appropriate mixture of MeOH in CH_2Cl_2 affording pure triazoles **8a–e**, respectively (for product characterization see Supporting Information).

Kinetic Measurements. The rate measurements of cycloaddition of cyclooctyne **1** with benzyl azide **10b** were conducted by using $^1\text{H NMR}$ spectroscopy (Varian Mercury 300 MHz) at 25°C . A 20 mM solution of benzyl azide **10b** (0.2 mL) in CDCl_3 :MeOD (4:1) was added to a thermally equilibrated solution of cyclooctyne **1** (10 mM, 0.4 mL) in a mixture of CDCl_3 :MeOD (4:1), leading to a mixture of both reactants in 1:1 ratio with a respective concentration of 6.66 mM. Reactions were monitored by following the decay of characteristic peaks of cyclooctyne **1** ($d = 3.78$ ($2 \times \text{OCH}_3$), 6.43 ($2 \times \text{CH}_{\text{Ar}}$) and 6.63 ($2 \times \text{CH}_{\text{Ar}}$) ppm) as well as the formation of characteristic triazole peaks ($d = 3.65$ (OCH_3), 3.89 (OCH_3), 5.43 (CH_2 -triazole) ppm). Consumption of starting materials followed a second-order equation and the second-order rate constants were obtained by least-squares fitting of the data to a linear equation (Figure S1).

Azido-BSA (9). A solution of *N*-[2-[(2-azidoethoxy)ethoxy]ethyl]-2-iodoacetamide **17** (50 mM, 0.6 mL) in a mixture of PBS buffer (20 mM, pH 7.3) and CH_3CN (1:1) was added to a solution of BSA (1 mM, 1 mL) in PBS buffer (20 mM, pH 7.3). The reaction mixture was shaken overnight at room temperature, dialyzed (MWCO = 10 kDa) against a mixture of PBS buffer (20 mM, pH 7.3) and CH_3CN (4:1) and stored at 4°C .

SPAAC with Azido-BSA. A solution of Fl-DIBO **1** (2.5 mM, 20 μL) in ethanol was added to a solution of azido-BSA **9** (50 μM , 180 μL) in PBS buffer (20 mM, pH 7.3, containing 1% SDS). The reaction mixture was incubated at 37°C overnight, separated by SDS-PAGE (10% gradient) and the gel was analyzed by fluorescence imaging ($\lambda_{\text{exc}} = 365$ nm; $\lambda_{\text{detec}} = 480$ nm) and by Coomassie Blue stain to reveal total protein content.

Absorption and Fluorescence Measurements. UV-vis spectra were recorded using Varian Cary Bio50 UV-vis spectrophotometer at $25 \pm 0.1^\circ\text{C}$. Fluorescence spectra were recorded with a PTI fluorimeter using a cuvette with 1 cm path length. All spectra were corrected for the spectral response of the detection system and for the spectral irradiance of the excitation source (via a calibrated photodiode). For spectra, see Supporting Information Figures S8–S13.

Quantum Yield Determination. Quantum yields were determined from the slope of the integrated fluorescence emission between 360 and 700 nm (excitation at 346 nm) versus absorbance using quinine sulfate ($\Phi_f = 0.54 \pm 0.03$) as fluorescence standard.⁴² For each compound, four data points were acquired with absorbances ranging between 0.05 and 0.5 ($l = 10$ cm).

Computational Studies. Quantum chemical calculations were carried out with the Gaussian 09 suite of programs (Rev. C01). All ground-state geometries were energy minimized by DFT with the B3LYP hybrid functional and Pople's 6-31G(d) split valence basis set with added polarization functions. In case of compound **1**, geometry

optimizations were performed within the C_{2v} point group. To ensure a stationary point on the ground-state potential surface, the optimized geometries were verified by a vibrational frequency analysis. Vertical excitation energies were calculated at the ground-state equilibrium geometry based on TD-DFT with the B3LYP or CAM-B3LYP³⁵ hybrid functionals and the 6-31+G(d) basis set with added diffuse functions. To estimate fluorescence emission energies, the geometry of the lowest excited state was optimized by TD-DFT at the B3LYP/6-31G(d) level of theory and the vertical emission energy was calculated at the excited state geometry (TD-DFT with B3LYP/6-31+G(d)). Bulk solvent effects were evaluated based on the polarizable continuum model (PCM) using default parameters.⁴³ For this purpose, ground state geometries were energy minimized with PCM equilibrium solvation (Tables S1 and S2), and the vertical excitation energies were subsequently calculated with ground-state solvation using TD-DFT in combination with B3LYP/6-31+G(d) or CAM-B3LYP/6-31+G(d), respectively. Similarly, fluorescence emission energies were obtained based on TD-DFT geometry optimizations with state-specific PCM equilibrium solvation,^{44,45} followed by a TD-DFT calculation with state-specific solvation using B3LYP/6-31+G(d) or CAM-B3LYP/6-31+G(d), respectively. Total electron density differences between the ground and excited states were visualized with VMD⁴⁶ based on Gaussian cube output files.

■ ASSOCIATED CONTENT

● Supporting Information

Synthetic procedures, kinetic data (Figure S1), stability studies (Figures S2–S6), solvatochromism (Figure S7), absorption and fluorescence spectra (Figures S8–S13), time-dependent fluorescence decay profiles (Figures S14–S18), computational studies (Tables S1–S4) and NMR spectra of synthesized compounds. This material is available free of charge via the Internet at <http://pubs.acs.org>.

■ AUTHOR INFORMATION

Corresponding Author

gjboons@ccrc.uga.edu

Notes

The authors declare no competing financial interest.

■ ACKNOWLEDGMENTS

Financial support from the National Institutes of Health (5R01CA088986, 5P41RR005351, and 8P41GM103390 to G.-J.B.) and (R01GM067169 to C.J.F.) is gratefully acknowledged.

■ REFERENCES

- (1) Crivat, G.; Taraska, J. W. *Trends Biotechnol.* **2012**, *30*, 8.
- (2) Lippincott-Schwartz, J.; Patterson, G. H. *Science* **2003**, *300*, 87.
- (3) Zhang, J.; Campbell, R. E.; Ting, A. Y.; Tsien, R. Y. *Nat. Rev. Mol. Cell Biol.* **2002**, *3*, 906.
- (4) Best, M. D.; Rowland, M. M.; Bostic, H. E. *Acc. Chem. Res.* **2011**, *44*, 686.
- (5) Jing, C.; Cornish, V. W. *Acc. Chem. Res.* **2011**, *44*, 784.
- (6) Sletten, E. M.; Bertozzi, C. R. *Angew. Chem., Int. Ed.* **2009**, *48*, 6974.
- (7) Debets, M. F.; van der Doelen, C. W. J.; Rutjes, F. P. J. T.; van Delft, F. L. *ChemBioChem* **2010**, *11*, 1168.
- (8) Schilling, C. I.; Jung, N.; Biskup, M.; Schepers, U.; Bräse, S. *Chem. Soc. Rev.* **2011**, 4840.
- (9) Saxon, E.; Bertozzi, C. R. *Science* **2000**, *287*, 2007.
- (10) Meldal, M.; Tornøe, C. W. *Chem. Rev.* **2008**, *108*, 2952.
- (11) Kennedy, D. C.; McKay, C. S.; Legault, M. C. B.; Danielson, D. C.; Blake, J. A.; Pegoraro, A. F.; Stolow, A.; Mester, Z.; Pezacki, J. P. *J. Am. Chem. Soc.* **2011**, *133*, 17993.

- (12) Soriano Del Amo, D.; Wang, W.; Jiang, H.; Besanceney, C.; Yan, A. C.; Levy, M.; Liu, Y.; Marlow, F. L.; Wu, P. *J. Am. Chem. Soc.* **2010**, *132*, 16893.
- (13) Debets, M. F.; van Berkel, S. S.; Dommerholt, J.; Dirks, A. T. J.; Rutjes, F. P. J. T.; van Delft, F. L. *Acc. Chem. Res.* **2011**, *44*, 805.
- (14) Jewett, J. C.; Bertozzi, C. R. *Chem. Soc. Rev.* **2010**, *39*, 1272.
- (15) Laughlin, S. T.; Baskin, J. M.; Amacher, S. L.; Bertozzi, C. R. *Science* **2008**, *320*, 664.
- (16) Ning, X.; Guo, J.; Wolfert, M. A.; Boons, G.-J. *Angew. Chem., Int. Ed.* **2008**, *47*, 2253.
- (17) Friscourt, F.; Ledin, P. A.; Mbua, N. E.; Flanagan-Steet, H. R.; Wolfert, M. A.; Steet, R.; Boons, G.-J. *J. Am. Chem. Soc.* **2012**, *134*, 5381.
- (18) Mbua, N. E.; Guo, J.; Wolfert, M. A.; Steet, R.; Boons, G.-J. *ChemBioChem* **2011**, *12*, 1912.
- (19) Debets, M. F.; van Berkel, S. S.; Schoffelen, S.; Rutjes, F. P. J. T.; van Hest, J. C. M.; van Delft, F. L. *Chem. Commun.* **2010**, 46, 97.
- (20) Jewett, J. C.; Sletten, E. M.; Bertozzi, C. R. *J. Am. Chem. Soc.* **2010**, *132*, 3688.
- (21) Poloukhina, A. A.; Mbua, N. E.; Wolfert, M. A.; Boons, G.-J.; Popik, V. V. *J. Am. Chem. Soc.* **2009**, *131*, 15769.
- (22) Canalle, L. A.; van Berkel, S. S.; de Haan, L. T.; van Hest, J. C. M. *Adv. Funct. Mat.* **2009**, *19*, 3464.
- (23) Kii, I.; Shiraishi, A.; Hiramatsu, T.; Matsushita, T.; Uekusa, H.; Yoshida, S.; Yamamoto, M.; Kudo, A.; Hagiwara, M.; Hosoya, T. *Org. Biomol. Chem.* **2010**, *8*, 4051.
- (24) Le Droumaguet, C.; Wang, C.; Wang, Q. *Chem. Soc. Rev.* **2010**, *39*, 1233.
- (25) Tobey, S. W.; West, R. *J. Am. Chem. Soc.* **1964**, *86*, 1459.
- (26) Dommerholt, J.; Schmidt, S.; Temming, R.; Hendriks, L. J.; Rutjes, F. P. J. T.; van Hest, J. C. M.; Lefeber, D. J.; Friedl, P.; van Delft, F. L. *Angew. Chem., Int. Ed.* **2010**, *49*, 9422.
- (27) van Geel, R.; Pruijn, G. J. M.; van Delft, F. L.; Boelens, W. C. *Bioconjugate Chem.* **2012**, *23*, 392.
- (28) Yao, J. Z.; Uttamapinant, C.; Poloukhina, A.; Baskin, J. M.; Codelli, J. A.; Sletten, E. M.; Bertozzi, C. R.; Popik, V. V.; Ting, A. Y. *J. Am. Chem. Soc.* **2012**, *134*, 3720.
- (29) Zhou, Z.; Fahrni, C. J. *J. Am. Chem. Soc.* **2004**, *126*, 8862.
- (30) Sivakumar, K.; Xie, F.; Cash, B. M.; Long, S.; Barnhill, H. N.; Wang, Q. *Org. Lett.* **2004**, *6*, 4603.
- (31) Sawa, M.; Hsu, T.-L.; Itoh, T.; Sugiyama, M.; Hanson, S. R.; Vogt, P. K.; Wong, C.-H. *Proc. Natl. Acad. Sci. U.S.A.* **2006**, *103*, 12371.
- (32) Lower, S. K.; Elsayed, M. A. *Chem. Rev.* **1966**, *66*, 199.
- (33) Reiser, A.; Marley, R. *Trans. Faraday Soc.* **1968**, *64*, 1806.
- (34) Silva-Junior, M. R.; Schreiber, M.; Sauer, S. P. A.; Thiel, W. *J. Chem. Phys.* **2008**, *129*, 104103.
- (35) Yanai, T.; Tew, D. P.; Handy, N. C. *Chem. Phys. Lett.* **2004**, *393*, 51.
- (36) Roos, B. In *Theoretical and Computational Chemistry. Vol 16. Computational Photochemistry*; Olivucci, M., Ed.; Elsevier: Boston, MA, 2005; Vol. 16, p 317.
- (37) Turro, N. J. *Modern Molecular Photochemistry*; University Science Books: Mill Valley, CA, 1991.
- (38) Gordon, C. G.; Mackey, J. L.; Jewett, J. C.; Sletten, E. M.; Houk, K. N.; Bertozzi, C. R. *J. Am. Chem. Soc.* **2012**, *134*, 9199.
- (39) Devaraj, N. K.; Hilderbrand, S.; Upadhyay, R.; Mazitschek, R.; Weissleder, R. *Angew. Chem., Int. Ed.* **2010**, *49*, 2869.
- (40) Lemieux, G. A.; De Graffenried, C. L.; Bertozzi, C. R. *J. Am. Chem. Soc.* **2003**, *125*, 4708.
- (41) Jewett, J. C.; Bertozzi, C. R. *Org. Lett.* **2011**, *13*, 5937.
- (42) Demas, J. N.; Crosby, G. A. *J. Phys. Chem.* **1971**, *75*, 991.
- (43) Tomasi, J.; Mennucci, B.; Cammi, R. *Chem. Rev.* **2005**, *105*, 2999.
- (44) Improta, R.; Barone, V.; Scalmani, G.; Frisch, M. J. *J. Chem. Phys.* **2006**, *125*, 054103.
- (45) Improta, R.; Scalmani, G.; Frisch, M. J.; Barone, V. *J. Chem. Phys.* **2007**, *127*, 074504.
- (46) Humphrey, W.; Dalke, A.; Schulten, K. *J. Mol. Graphics Modell.* **1996**, *14*, 33.